Applied Surface Science 518 (2020) 146218

Contents lists available at ScienceDirect

Applied Surface Science

journal homepage: www.elsevier.com/locate/apsusc

Full Length Article

Growth of high-quality AlN films on sapphire substrate by introducing voids through growth-mode modification

Bin Tang[a,1], Hongpo Hu[a,1], Hui Wan[b,1], Jie Zhao[a], Liyan Gong[a], Yu Lei[a], Qiang Zhao[b], Shengjun Zhou[a,b,c,*]

[a] Center for Photonics and Semiconductors, School of Power and Mechanical Engineering, Wuhan University, Wuhan 430072, China
[b] The Institute of Technological Sciences, Wuhan University, Wuhan 430072, China
[c] State Key Laboratory of Applied Optics, Changchun Institute of Optics, Fine Mechanics and Physics, Chinese Academy of Sciences, Changchun 130033, China

ARTICLE INFO

Keywords:
AlN
Void
Dislocation
Stress relaxation

ABSTRACT

We demonstrate the achieving of high-quality AlN films on flat sapphire substrate (FSS) by introducing voids during growth. Voids are embedded into AlN epilayers through a growth-mode transition from island growth to step flow growth. Such voids significantly facilitated the underlying dislocations annihilation as demonstrated by the transmission electron microscopy (TEM) image. For the 3 μm-thick AlN film grown on FSS, the full width at half maximum of the X-ray rocking curve was 57/260 arcsec for (0 0 2)/(1 0 2) reflection and a threading dislocation density of 1.7×10^8 cm^{-2} was determined from plain-view TEM image. Moreover, the voids provided an additional stress relief channel in the AlN film grown on FSS, resulting in a tensile stress comparable to that of grown on nano-patterned sapphire substrate (NPSS). The measured lattice constants and Raman shift of AlN-E_2 (high) peak verified the 3 μm-thick AlN film grown on FSS is nearly stress free at room temperature. Taking advantages of the deliberately embedded voids, a crack-free and atomically flat AlN film was grown on FSS. The strategy put forward in this work to obtaining high-quality AlN films on FSS is much cost-efficient, which is believed to hold great promise for commercialization in AlN-based devices.

1. Introduction

The epitaxial growth of high-quality AlN films is essential for high-efficiency deep-ultraviolet (DUV) optoelectronic devices [1–3], such as light-emitting diodes (LEDs) [4–6], laser diodes (LDs) [7], and high-frequency power electronics [8–10]. Owing to the lack of economic AlN bulk substrate, AlN films are usually obtained by epitaxially grown on foreign substrates through metal-organic chemical vapor deposition (MOCVD) method [11–13]. Sapphire is the preferred substrate for AlN epitaxy because of its low cost and transparency to UV light [14,15]. However, due to the large mismatch in lattice constants and thermal expansion coefficients (TEC) between AlN and sapphire, the epitaxial AlN films suffering from severe stresses are generally with high density of threading dislocations (10^9 –10^{10} cm^{-2}) [16–18]. These defects can significantly degrade the device performance by acting as non-radiative recombination centers or leakage current pathway [19,20]. Moreover, AlN cracking will be induced by the large tensile stress, which is a major concern for the device reliability issue.

Several approaches have been explored to improve the epitaxial quality of AlN on sapphire. High growth temperature (over 1300 °C) has been adopted to enhance the migration of Al adatoms for an atomically flat AlN surface [21,22]. In addition, high temperature annealing (1700 °C) in N_2 + CO ambient was demonstrated to significantly reduce the threading dislocation density (TDD) [23]. However, AlN films grown on sapphire suffer from increasing risk of cracking at such high temperature and achieving these high temperature conditions always require specially designed reactor which increases the manufacturing cost. Sapphire offcut and surface pretreatments were also investigated to improve the crystal quality [24–26]. Nonetheless, precise control of the sapphire surface is difficult and additional substrate processing steps are costly. Recently, by taking advantages of nanoscale epitaxial lateral overgrowth (ELOG), AlN grown on nano-patterned sapphire substrate (NPSS) has attracted much research interest [27–29]. The coalescence of AlN films on NPSS always embeds voids into the epilayers, which are critical to the crystal quality improvement by playing the role of dislocation filter and additional stress relief channel. However, in order to achieve nanoscale patterns on sapphire substrates, the surface patterning processes of NPSSs

* Corresponding author at: Center for Photonics and Semiconductors, School of Power and Mechanical Engineering, Wuhan University, Wuhan 430072, China.
E-mail address: zhousj@whu.edu.cn (S. Zhou).
[1] B. Tang, H. Hu, and H. Wan contributed equally to this work.

https://doi.org/10.1016/j.apsusc.2020.146218
Received 1 December 2019; Received in revised form 23 March 2020; Accepted 26 March 2020
Available online 27 March 2020
0169-4332/

usually involve sophisticated and costly photolithography procedure.

In this work, we successfully brought voids into AlN films grown on flat sapphire substrate (FSS) through a growth-mode modification process, which enabled the realization of high quality, crack-free AlN films on FSS. Dislocations termination at the void sidewalls are observed, verifying the practicability of introducing voids for dislocation filtering in the epitaxial growth of AlN on FSS. Moreover, we believed that the voids were responsible for an observed drastic decrease of tensile stress from 1.34 GPa to 0.44 GPa during growth. With the introducing of voids, the 3 μm-thick AlN film grown on FSS demonstrated a low TDD of 1.7×10^8 cm^{-2} and was nearly free of residual stress. Compared to the patterned substrates based ELOG process, our work provides a much more cost-efficient way to achieving high-quality AlN film, which largely promotes the prospect of commercial AlN-based devices.

2. Experiments

AlN films were heteroepitaxially grown on 2-*inch* FSS and NPSS by using an AIXTRON Crius I close-coupled showerhead reactor MOCVD system. The NPSS used in this study is featured with hexagonally arranged holes as shown in Fig. 1a. The period, diameter, and depth of dimples are 1 μm, 900 nm, and 500 nm, respectively. AlN epilayers grown on the sapphire substrates take the epitaxial relationship of AlN (0 0 0 2)//Al_2O_3(0 0 0 6) and AlN(1 − −1 0 0)//Al_2O_3(1 1 − −2 0), which were confirmed by the selected area electron diffraction (SAED) pattern from AlN/sapphire interface region (Fig. 1b). Structures and growth procedures of the AlN epilayers on FSS and NPSS are schematically illustrated in Fig. 1c. The growth of AlN epilayers was started with the deposition of 20 nm-thick AlN nucleation layer (NL) on FSS and NPSS using a NMC iTops A330 sputtering system. A 2-*inch* Al disk (99.999%) was used as sputtering target for the reactively sputtering deposition of AlN NL in argon-nitrogen atmosphere. The deposition process was performed at 650 ˚C by feeding 120 sccm N_2, 30 sccm Ar, and 1 sccm O_2. Trimethyl aluminum (TMAl) and ammonia (NH_3) were used as Al and N precursors for the MOCVD growth, respectively. During the MOCVD growth process, hydrogen (H_2) was used as the carrier gas and the reactor pressure was kept at 50 mbar. The substrates with sputtered AlN NL were first thermally preheated at 850 ˚C for 5 min in the chamber. Subsequently, a 180 nm-thick high-temperature AlN (HT AlN-1) layer was grown at 1200 ˚C with V/III ratio of 3350, followed by the growth of a 270 nm-thick low-temperature AlN (LT AlN) layer at 960 ˚C. Afterward, a 450 nm-thick AlN layer was grown at 1200 ˚C using pulsed atomic-layer epitaxy (PALE) method to ensure a fast coalescence of the *c*-plane surface. For the growth of PALE AlN layer, the NH_3 flow was alternatively turned on/off (5-sec/5-sec), while the TMAl flow was kept continuous. Finally, the V/III ratio was ramped down to 190 for a fast growth of 2.1 μm-thick HT AlN-2 layer at 1200 ˚C. For clarification, the growth process was denoted as stages S1-S4 in sequence as shown in Fig. 1c.

In-situ reflectance monitoring was performed using a Laytec EpiTT system acquiring reflectance signal at 405 nm. Emissivity corrected pyrometry (true temperature) was used to estimate the temperature during growth and a Laytec EpiCurve system was used to measure wafer curvature at the wafer center. Surface morphology characterization was conducted using a TESCAN MIRA 3 LMH field emission scanning electron microscope (SEM) and a JPK NanoWizard 4 atomic force microscopy (AFM). High-resolution X-ray diffraction (HRXRD)

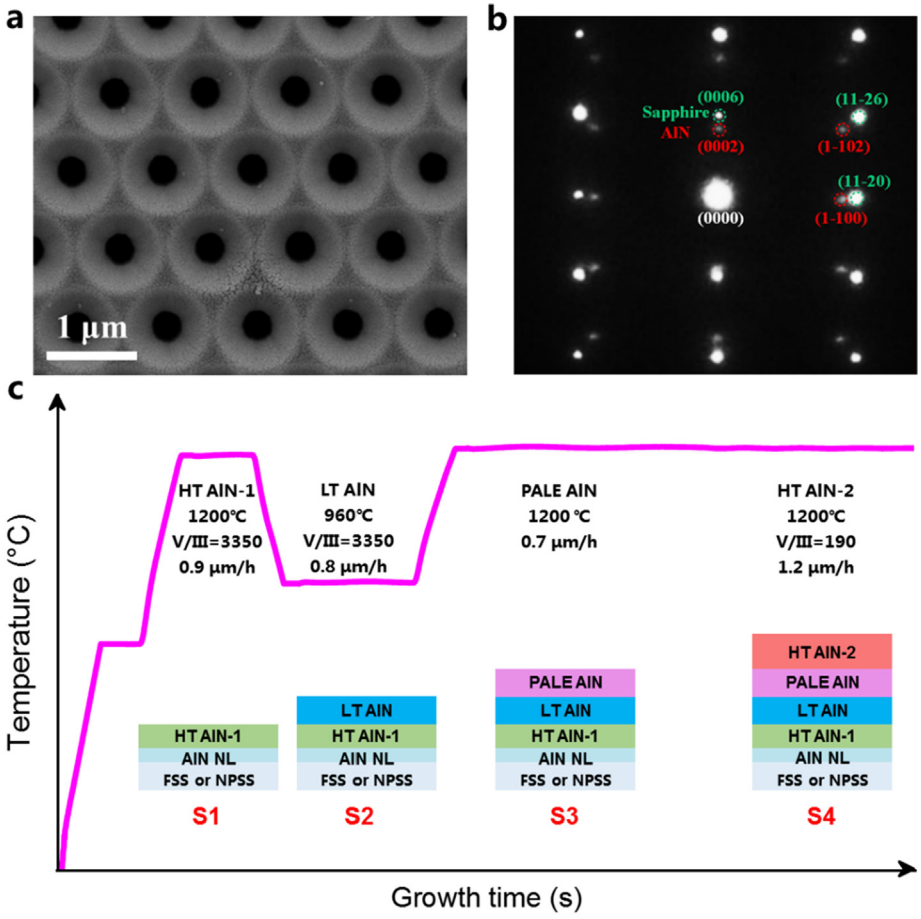

Fig. 1. (a) A top-view SEM image of the NPSS used in this study. (b) SAED pattern of the AlN/sapphire interface region. (c) The growth procedures of AlN on FSS or NPSS.

measurements were performed using a PAnalytical X'Pert Pro MRD diffractometer. All measurements of rocking curves were based on a typical double-crystal X-ray diffraction mode [30]. For the incident optics unit, a Ge(2 2 0) 2-bounce monochromator was adopted. As for the receiving optics unit, we did not add any analysis crystal except for two inherent slits. Crystal structure and defect analysis was performed using a FEI Tecnai F20 scanning transmission electron microscope (STEM). Micro-Raman measurements were conducted at room temperature by a Renishaw Raman system with the 514 nm Ar^+-laser laser as the excitation source. The laser beam was focused with a microscope lens ($\times$80, NA = 0.75) to about 0.75 μm spot diameter on the sample surface. The scattered light was dispersed through the monochromator system attached to a liquid nitrogen cooled charge coupled detector (CCD) detector. The spectrometer was calibrated carefully using the silicon Raman mode and the laser plasma lines. Overall spectral resolution and accuracy during the Raman measurements was better than 0.2 cm^{-1}.

3. Results and discussion

First, reflectance transients during the whole AlN growth process were *in-situ* monitored to provide information on surface morphology evolution (as shown in Fig. 2a). In the reflectance profiles, the Fabry-Pérot oscillations are indicative of increasing AlN layer thickness and the ascent/descent of the oscillation amplitude implies surface smoothing/roughening. A lower initial reflectance was observed for the NPSS sample due to its inherent rough patterned surface. The reflectance profiles started to oscillate with the growth of AlN films. The growth of HT AlN-1 layer (stage S1) on either FSS or NPSS induced slight decrease of the oscillation amplitude, suggesting the roughening of surface morphology. During the growth of LT AlN layer (stage S2), the oscillation amplitude of AlN/FSS drops sharply and it was kept at a very low level for AlN/NPSS since the three-dimensional (3D) island growth at low temperature further roughened sample surface. By introducing of PALE AlN layer (stage S3), the oscillation amplitudes of both AlN/FSS and AlN/NPSS quickly rise up with the coalescence of island grains. AlN/NPSS showed a slower coalescence speed than AlN/FSS as indicated by the later appearance of maximum reflectance intensity. By the end of the growth process, both the AlN/FSS and AlN/NPSS films showed smooth and uniform surface morphology as observed under Normarski interference optical microscope images (Fig. 2b and 2c).

We carried out growth interruption experiments to investigate the morphology evolution of AlN epilayers. The SEM images in Fig. 3 show the representative surface morphologies of AlN/ FSS and AlN/NPSS at different growth stages, which reveal the growth mode transitions of AlN in the whole growth process. During stage S1, the smooth AlN *c*-plane surface gradually reduced owing to preferred vertical growth under high V/III ratio (3350), resulting in the descent of reflectance intensity as shown in Fig. 2a. The following growth of LT AlN at stage S2 involved high density of pits on the surface owing to 3D island growth, which further reduced the smooth *c*-plane surface. We set a low temperature (960 °C) and high V/III ratio (3350) growth parameter at this stage to produce pits with a large depth/width ratio. At stage S3, diffusion length of Al adatoms were largely prolonged by the PALE growth mothed, which provided a rapid coalescence speed of the *c*-

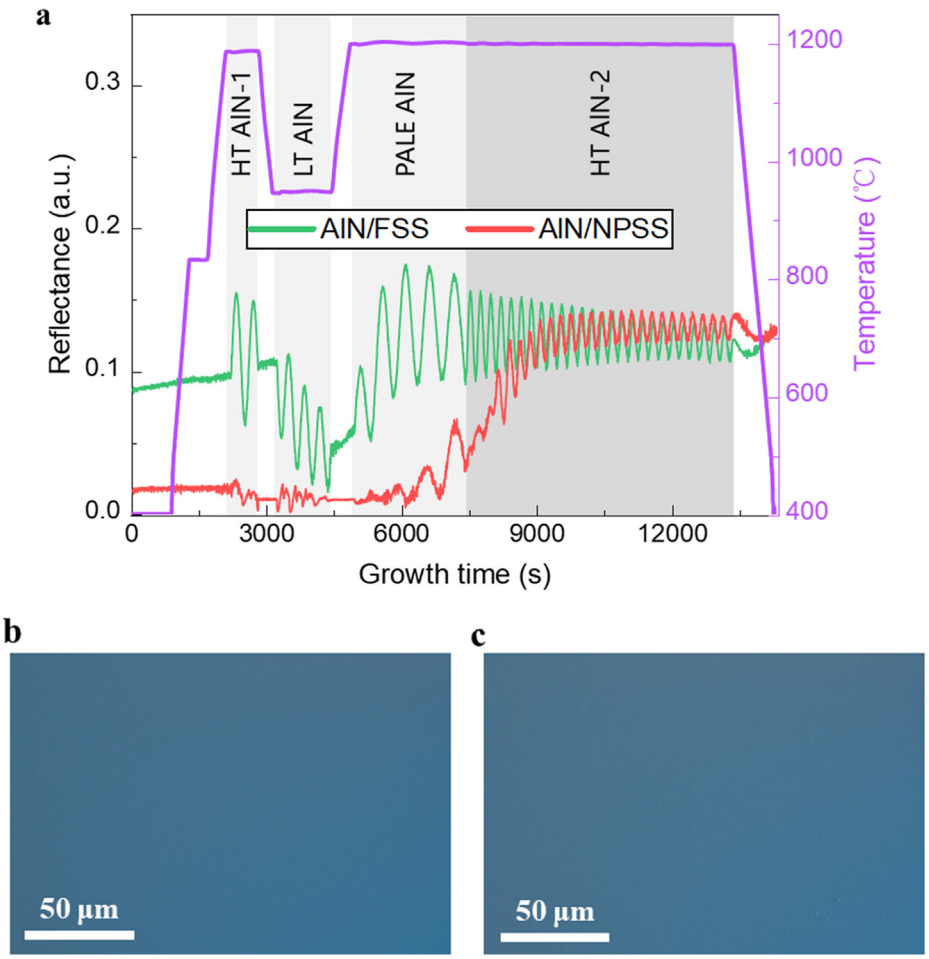

Fig. 2. (a) *In-situ* reflectance monitoring of AlN growth with 405 nm light source, which provides information on growth rate and morphological development in real time. Normarski interference optical microscope image of the AlN film grown on (b) FSS and (c) NPSS.

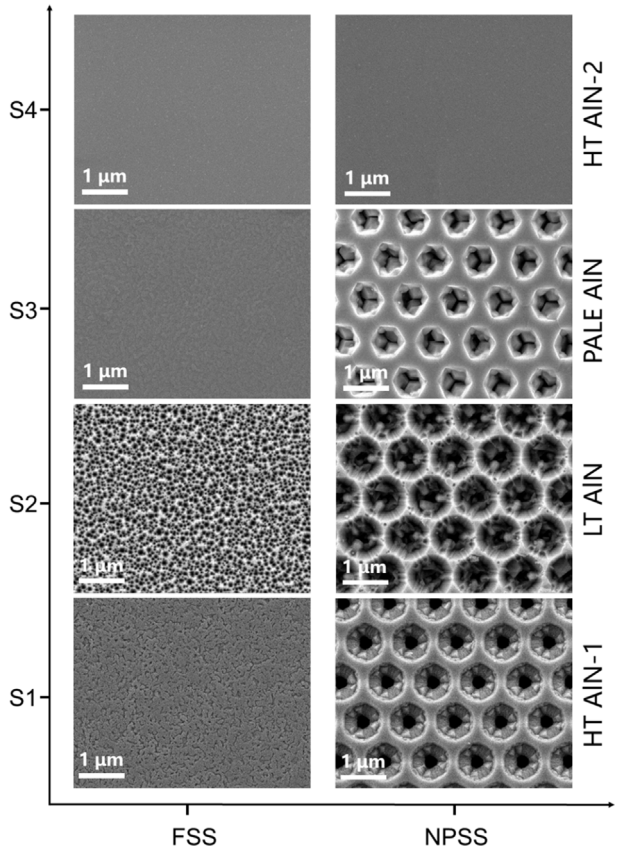

Fig. 3. Surface morphologies of AlN/FSS and AlN/NPSS, showing their evolution of growth from initial to latter growth stages.

plane surface. After the growth of 450 nm-thick PALE AlN, the AlN/FSS achieved a fully coalesced surface, while the coalescence of AlN/NPSS was incomplete. This agrees with the location of their maximum reflectance intensities in the *in-situ* reflectance profiles as shown in Fig. 2a. When the following growth of a 2.1 μm-thick HT AlN-2 layer was completed, both AlN/FSS and AlN/NPSS showed smooth top surface. AFM measurements were conducted to characterize the final surface morphologies (Fig. 4). Atomically flat surface of AlN with straight parallel steps and terraces are observed for both AlN/FSS and AlN/NPSS, indicating the dominant step-flow growth at stage S4. The height of steps is in the range of 0.20–0.30 nm, corresponding to one monolayer of (0 0 0 1) AlN (c/2 = 0.25 nm). Root mean square (RMS) roughness of AlN/FSS and AlN/NPSS are 0.263 nm and 0.248 nm over the scan area of 2 × 2 μm^2, respectively. Overall, the above results demonstrated that AlN/FSS achieved an atomically flat and crack-free surface after the four-step growth process, which is comparable with that of AlN/NPSS. In contrast, crack formation takes place already due to the large tensile stress for the AlN layer with thicknesses over 1 μm in previous publications [27,31].

Cross-sectional view of the AlN films using STEM was performed to show voids embedded in AlN/FSS films during MOCVD growth. The STEM samples were cut in the (1 0 − −1 0) zone axes. Fig. 5a and 5b showed the STEM images of AlN/FSS and AlN/NPSS taken under 2-beam condition in the $\boldsymbol{g}$ = (1 1 − −1 0) direction, where the edge and mixed type dislocations were visible. For both AlN/FSS and AlN/NPSS, hh density of dislocations were generated at the AlN/sapphire interface to accommodate the large lattice mismatch (lattice constants: a_{AlN} = 0.3112 nm, $a_{sapphire}$ = 0.4758 nm) [16]. Most of the dislocations in AlN/NPSS quickly annihilated, which benefited from the nanoscale width of the growth mesa. However, the majority of dislocations in AlN/FSS remained propagating upward after the growth of HT AlN-1 layer. Although dislocation reduction occurred throughout the growth of LT AlN layer in AlN/FSS, the STEM images demonstrated a much larger TDD in AlN/FSS (than that in AlN/NPSS) with the accomplishment of LT AlN layer. For AlN/FSS sample, dislocations suffered from a significant annihilation with the growth of PALE AlN layer and plenty of voids embedded in this layer was observed. An enlarged view of the void showed that there existed dislocation termination at void sidewalls and the nucleation of new dislocations at the coalescence boundary of void (Fig. 5c). Void-structures are widely observed in AlN films grown on patterned substrates owing to the epitaxial lateral overgrowth (ELOG) [32], just as observed in AlN/NPSS (Fig. 5b). It is believed that such void-structures not only facilitate dislocation annihilation but also provide an additional stress relief channel, which contribute to the realization of high-quality AlN films on NPSS. However, such void structures are rarely observed in AlN film grown on FSS. Here, voids are deliberately introduced in AlN/FSS with the intention of filtering dislocation and releasing stress. It can be observed from the STEM images that dislocations in AlN/FSS annihilated to a level comparable to that in AlN/NPSS over the voids. Based on the STEM images and growth interruption experiments, we proposed a possible model to illustrate the dislocation behavior in AlN/FSS, as shown in Fig. 5d. At initial stage (S1), the dislocations arising from AlN/sapphire interface thread through the HT AlN-1 layer. It is likely that the 3D island growth at stage S2 facilitates dislocations bending to react with adjacent dislocations. Hence, dislocation fusion and annihilation reactions occurred in LT AlN layer. At stage S3, the fast coalescence of 3D islands embedded voids into the PALE AlN layer. Once upward propagating dislocations come across these voids, they may be subject to the images forces imposed by void sidewalls, thus enabling the termination of dislocations. Besides, there also occurs the nucleation of dislocations at the coalescence boundary above a void. Benefiting from the dislocations filtering by voids, few dislocations finally thread to the film surface after employing the thick HT AlN-2 layer.

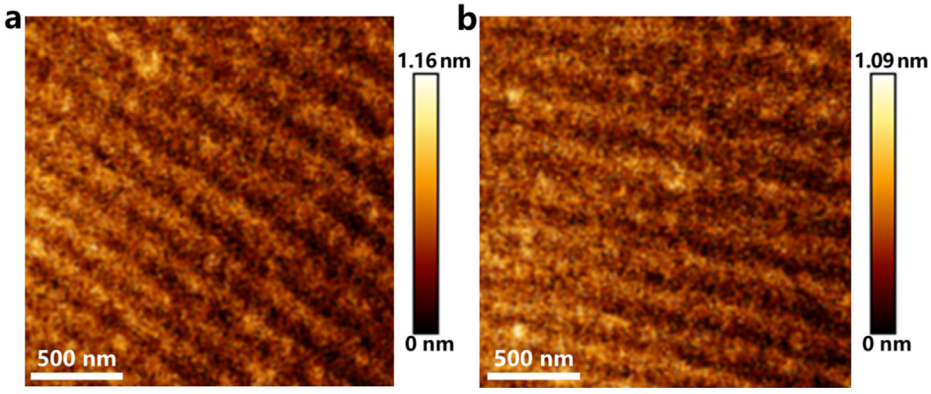

Fig. 4. AFM images of (a) AlN/FSS and (b) AlN/NPSS, showing their final surface morphologies.

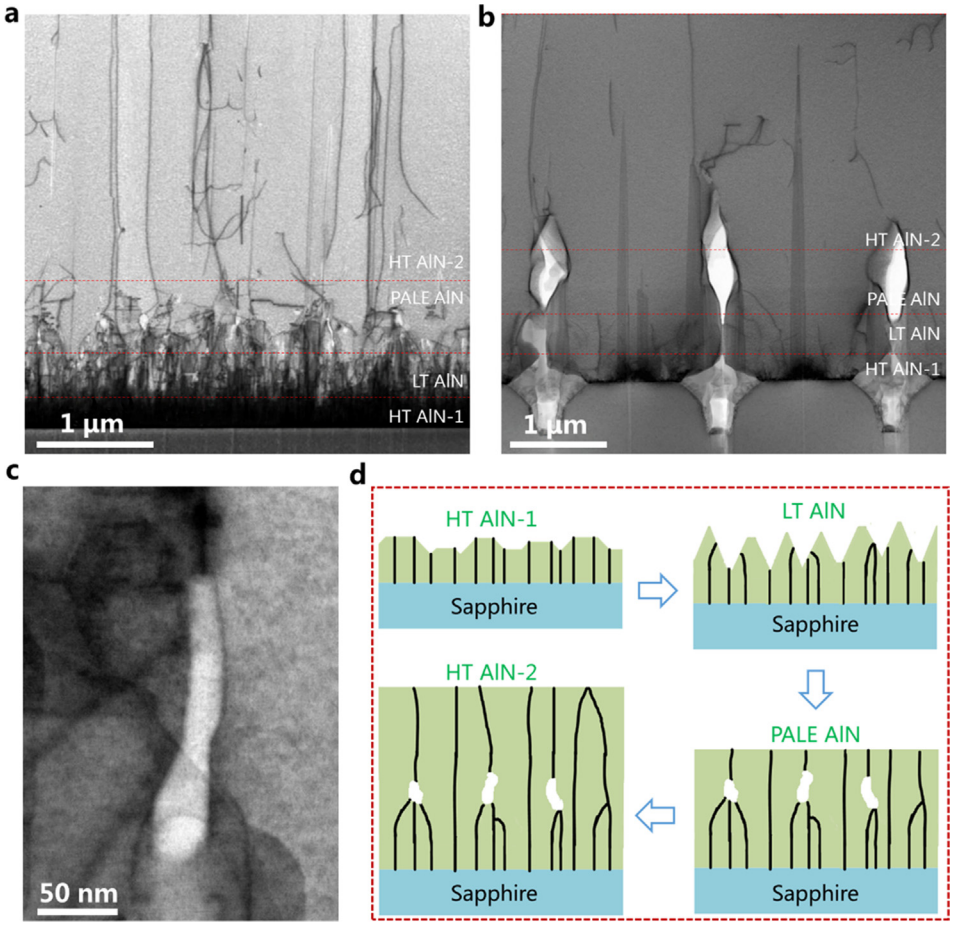

Fig. 5. AlN films cut in the (1 0 − −1 0) zone axis and tilted to the $\boldsymbol{g}$ = (1 1 − −2 0) direction: (a) AlN/FSS (b) AlN/NPSS and (c) an enlarged view of the void in AlN/FSS. (d) A possible model of the dislocation behavior in AlN/FSS.

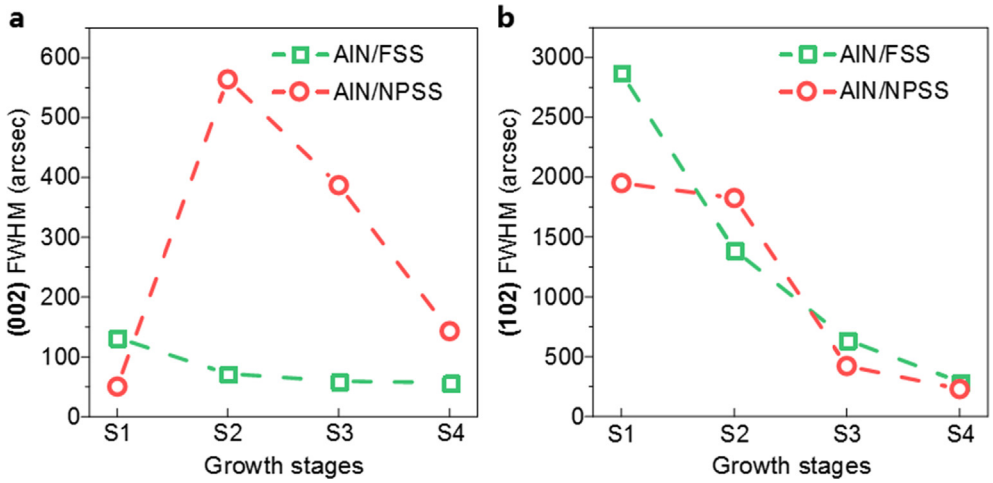

Fig. 6. (a) FWHM of (0 0 2) reflection peak for AlN/FSS and AlN/NPSS at different stages. (b) FWHM of (1 0 2) reflection peak for AlN/FSS and AlN/NPSS at different stages.

The HRXRD rocking curve measurements were performed to evaluate the crystal quality of AlN films at different growth stages. It can be observed in Fig. 6 that the FWHMs of (0 0 2) and (1 0 2) reflection peaks for AlN/FSS monotonously declines from stages S1 to S4, evidencing the reduction of TDD. We also find that the FWHMs of AlN/NPSS are anomalously high at stages S1 and S2, which is believed to arise from misaligned crystallites that grow on the pattern sidewall of NPSS [22]. The final FWHMs of (0 0 2)/(1 0 2) reflection peaks for AlN/FSS and AlN/NPSS are 57/260 and 143/211 arcsec, respectively. TDD evaluated from the HRXRD method is generally overestimated, since there can be more rocking curve broadening mechanisms presenting than only dislocations, e.g., wing tilt due to lateral growth over voids, wafer curvature [33]. Hence, plan-view STEM measurements were carried out to give a more accurate quantitative evaluation of TDDs. Plan-view STEM measurements were conducted under 2-beam diffraction condition in $\boldsymbol{g}$ = (1 1 − −2 0) direction. The AlN samples were

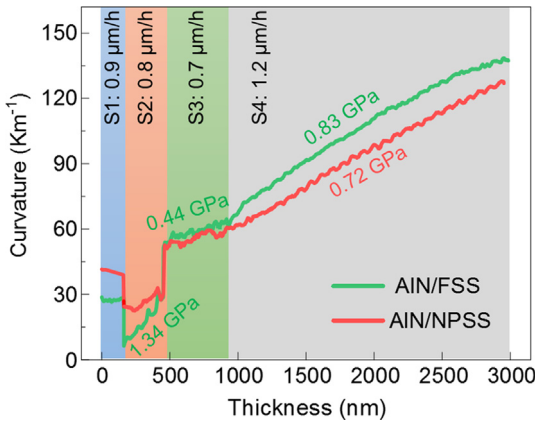

Fig. 7. *In-situ* wafer curvature as a function of AlN film thickness.

tilted 18° from [0 0 0 1] direction to detect all three dislocation types (edge, screw, and mixed) at the same time [34]. As shown in Figure S1, dislocations in AlN/FSS and AlN/NPSS are imaged owing to the strain field contrast around them. According to the selected areas (~45 μm^2), the TDDs in AlN/FSS and AlN/NPSS are 1.7 × 10^8 and 9.8 × 10^7 cm^{-2}, respectively.

Wafer bowing and cracking are common problems in the epitaxial growth of AlN on sapphire substrate due to the thermal expansion coefficient mismatch and the intrinsic tensile stress which develops during growth. Typically, for AlN film grown on FSS, cracks are observed when the thickness of AlN is increased to 1 μm [27,31]. In this work, we obtained a 3 μm-thick crack-free AlN film on FSS. *In–situ* wafer curvature variation was monitored to show the in-plane stress evolution during AlN growth (Fig. 7). According to Stoney's Equation [35], there exists the relationship between substrate curvature (κ) and in-plane film stress (σ_f):

$$\sigma_f h_f = \frac{M_s h_s^2}{6}\kappa \tag{1}$$

where h_f is film thickness, h_s is the substrate thickness and M_s is the substrate biaxial modulus. Hence, the in-plane stress can be obtained according to the transformation of

Stoney's Equation:

$$\frac{d\kappa}{dh_f} = \frac{6\sigma_f}{M_s h_s^2} \tag{2}$$

An average tensile stress of 1.34 GPa in AlN/FSS during stage S2 (at 960 °C, 0.8 μm/h) was determined from the curvature-thickness plot. The average tensile stress in AlN/FSS sharply dropped to 0.44 GPa during stage S3 (at 1200 °C, 0.7 μm/h) and reached 0.83 GPa during stage S4 (at 1200 °C, 1.2 μm/h). Sheldon *et al.* has developed a kinetic model to interpret the stress evolution during film growth [36,37]. The model describes the competition between compressive and tensile mechanisms. For AlN films epitaxy on sapphire, the thermal expansion mismatch is partly responsible for the compressive mechanisms, while morphological evolution consisting of grain coalescence, lateral grain growth and dislocation inclination is expected to be responsible for tensile mechanisms [38,39]. The increased tensile stress from S3 to S4 can be well explained by the competition model as the larger growth rate of stage S4 favors the tensile mechanisms. The decreased growth rate from S2 to S3 is responsible for the observed decrease in tensile stress according to the competition model. However, we suggested that it is not the only answer to such a drastic decrease, especially when considering the stress evolution from S3 to S4. The embedded voids are believed to play an important role for the stress evolution in AlN/FSS, resulting in a stress comparable to that in AlN/NPSS during stage S4.

The lattice constants *a* and *c* at different growth stages were determined from *ex-situ* HRXRD 2θ-ω scans by measuring the (0 0 2) and (1 0 5) reflection peaks (Fig. 8a). The lattice constants suggested that both AlN/FSS and AlN/NPSS were under compressive stress at room temperature after each growth stage, which was mainly arising from the lattice mismatch between AlN and sapphire. Residual stresses were also characterized by Raman spectra according to the stress-sensitive AlN-E_2 (high) peaks (Fig. 8b), which demonstrated a consistent tendency of the stress evolution with the lattice constants. The compressive stress in AlN/FSS underwent a continuous relaxation during the four-step growth. After the accomplishment of the growth process, the E_2 (high) peak of AlN/FSS was located at 657.5 cm^{-1}, close to that of stress-free AlN (657.4 cm^{-1}) [40]. A residual compressive stress of 33 MPa for the AlN/FSS film was determined from the Raman shift, which suggests the compressive stress caused by lattice mismatch is significantly relaxed.

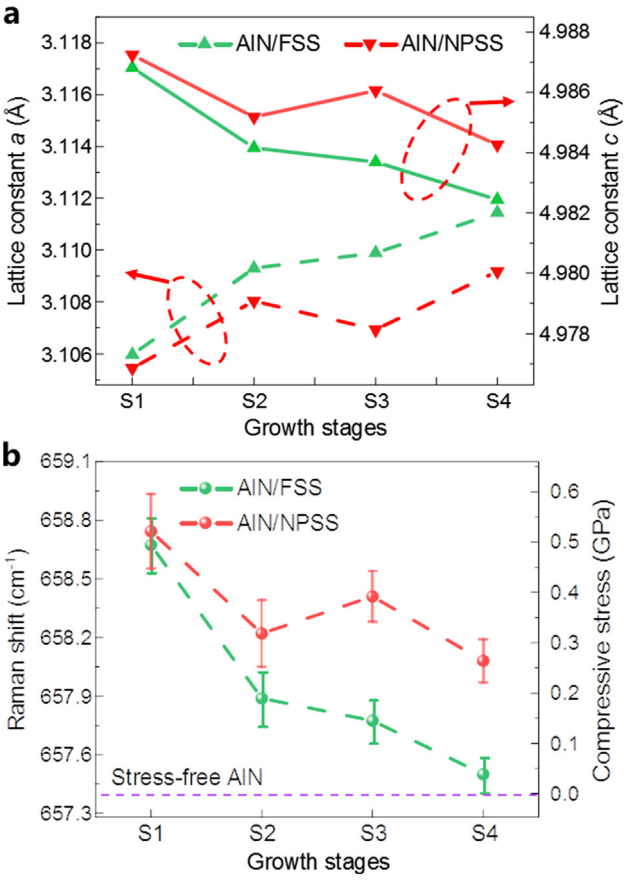

Fig. 8. (a) The lattice constants of AlN/FSS and AlN/NPSS at different growth stages determined from HRXRD 2θ-ω scans. (b) The Raman shift of stress-sensitive AlN-E_2 (high) peak and calculated residual stress of AlN/FSS and AlN/NPSS.

4. Conclusions

In summary, the success of introducing voids into AlN film grown on FSS for dislocation filter and strain relief was demonstrated. We show that dislocation annihilation in the AlN film grown on FSS was facilitated by the embedded voids, resulting in a low TDD of 1.7 × 10^8 cm^{-2} in the 3 μm-thick AlN film. Furthermore, with the introduction of voids into the AlN film grown on FSS, a drastic drop of the *in-situ* tensile stress from 1.34 GPa to 0.44 GPa was observed, which reduced the risk of cracking. Taking advantages of the embedded voids, nearly stress free AlN films with atomically flat surface were grown on FSS. In comparison with the strategy of ELOG on patterned substrates, our approach is much more cost-efficient and hence hold great promise for the application in mass-production.

CRediT authorship contribution statement

Bin Tang: Conceptualization, Investigation, Writing - original draft. **Hongpo Hu:** Validation, Investigation, Writing - review & editing. **Hui Wan:** Writing - review & editing. **Jie Zhao:** Visualization, Writing - review & editing. **Liyan Gong:** Visualization, Writing - review & editing. **Yu Lei:** Visualization, Writing - review & editing. **Qiang Zhao:** Writing - review & editing. **Shengjun Zhou:** Conceptualization, Supervision, Writing - review & editing.

Declaration of Competing Interest

The authors declare that they have no known competing financial interests or personal relationships that could have appeared to influence the work reported in this paper.

Acknowledgements

This work was supported by the National Natural Science Foundation of China (51675386, U1501241, and 51775387), Natural Science Foundation of Hubei Province (2018CFA091), and the National Key Research and Development Program of China (2017YFB1104900).

Appendix A. Supplementary material

Supplementary data to this article can be found online at https://doi.org/10.1016/j.apsusc.2020.146218.

References

[1] Y. Chen, Z. Zhang, H. Jiang, Z. Li, G. Miao, H. Song, The optimized growth of AlN templates for back-illuminated AlGaN-based solar-blind ultraviolet photodetectors by MOCVD, J. Mater. Chem. C 6 (2018) 4936–4942.
[2] M. Kneissl, T.Y. Seong, J. Han, H. Amano, The emergence and prospects of deep-ultraviolet light-emitting diode technologies, Nat. Photonics 13 (2019) 233–244.
[3] S. Zhao, M. Djavid, Z. Mi, Surface Emitting, high efficiency near-vacuum ultraviolet light source with aluminum nitride nanowires monolithically grown on silicon, Nano Lett. 15 (2015) 7006–7009.
[4] N. Susilo, S. Hagedorn, D. Jaeger, H. Miyake, U. Zeimer, C. Reich, B. Neuschulz, L. Sulmoni, M. Guttmann, F. Mehnke, C. Kuhn, T. Wernicke, M. Weyers, M. Kneissl, AlGaN-based deep UV LEDs grown on sputtered and high temperature annealed AlN/sapphire, Appl. Phys. Lett. 112 (2018) 041110.
[5] Z. Chen, Z. Liu, T. Wei, S. Yang, Z. Dou, Y. Wang, H. Ci, H. Chang, Y. Qi, J. Yan, J. Wang, Y. Zhang, P. Gao, J. Li, Z. Liu, Improved epitaxy of AlN film for deep-ultraviolet light-emitting diodes enabled by graphene, Adv. Mater. 31 (2019) 1807345.
[6] H. Hu, B. Tang, H. Wan, H. Sun, S. Zhou, J. Dai, C. Chen, S. Liu, L.J. Guo, Boosted ultraviolet electroluminescence of InGaN/AlGaN quantum structures grown on high-index contrast patterned sapphire with silica array, Nano Energy 69 (2020) 104427.
[7] R. Ni, X. Chen, J. Yan, L. Zhang, Y. Guo, J. Wang, J. Li, Y. Zhang, Reducing stimulated emission threshold power density of AlGaN/AlN multiple quantum wells by nano-trench-patterned AlN template, J. Alloy. Compd. 777 (2019) 344–349.
[8] S. Muhtadi, S.M. Hwang, A. Coleman, F. Asif, G. Simin, M.V.S. Chandrashekhar, A. Khan, High electron mobility transistors with Al0.65Ga0.35N channel layers on thick AlN/Sapphire templates, IEEE Electron Device Lett. 38 (2017) 914–917.
[9] U.K. Mishra, P. Parikh, Y.F. Wu, AlGaN/GaN HEMTs – an overview of device operation and applications, Proc. IEEE 90 (2002) 1022–1031.
[10] X. Wang, R. Yu, C. Jiang, W. Hu, W. Wu, Y. Ding, W. Peng, S. Li, Z.L. Wang, Piezotronic effect modulated heterojunction electron gas in AlGaN/AlN/GaN heterostructure microwire, Adv. Mater. 28 (2016) 7234–7242.
[11] D.D. Koleske, J.J. Figiel, D.L. Alliman, B.P. Gunning, J.M. Kempisty, J.R. Creighton, A. Mishima, K. Ikenaga, Metalorganic vapor phase epitaxy of AlN on sapphire with low etch pit density, Appl. Phys. Lett. 110 (2017) 232102.
[12] L. Huang, Y. Li, W. Wang, X. Li, Y. zheng, H. Wang, Z. Zhang, G. Li, Growth of high-quality AlN epitaxial film by optimizing the Si substrate surface, Appl. Surf. Sci. 435 (2018) 163–169.
[13] C.J. Zollner, A. Almogbel, Y. Yao, B.K. SaifAddin, F. Wu, M. Iza, S.P. DenBaars, J.S. Speck, S. Nakamura, Reduced dislocation density and residual tension in AlN grown on SiC by metalorganic chemical vapor deposition, Appl. Phys. Lett. 115 (2019) 161101.
[14] S. Zhou, X. Liu, H. Yan, Z. Chen, Y. Liu, S. Liu, Highly efficient GaN-based high-power flip-chip light-emitting diodes, Opt. Express 27 (2019) A669–A692.
[15] S. Zhou, H. Xu, H. Hu, C. Gui, S. Liu, High quality GaN buffer layer by isoelectronic doping and its application to 365 nm InGaN/AlGaN ultraviolet light-emitting diodes, Appl. Surf. Sci. 471 (2019) 231–238.
[16] Y. Qi, Y. Wang, Z. Pang, Z. Dou, T. Wei, P. Gao, S. Zhang, X. Xu, Z. Chang, B. Deng, S. Chen, Z. Chen, H. Ci, R. Wang, F. Zhao, J. Yan, X. Yi, K. Liu, H. Peng, Z. Liu, L. Tong, J. Zhang, Y. Wei, J. Li, Z. Liu, Fast Growth of Strain-Free AlN on Graphene-Buffered Sapphire, J. Am. Chem. Soc. 140 (2018) 11935–11941.
[17] V. Jindal, F. Shahedipour-Sandvik, Density functional theoretical study of surface structure and adatom kinetics for wurtzite AlN, J. Appl. Phys. 105 (2009) 084902.
[18] X.-H. Li, S. Wang, H. Xie, Y.O. Wei, T.-T. Kao, M.M. Satter, S.-C. Shen, P. Douglas Yoder, T. Detchprohm, R.D. Dupuis, A.M. Fischer, F.A. Ponce, Growth of high-quality AlN layers on sapphire substrates at relatively low temperatures by metal-lorganic chemical vapor deposition, Phys. Status Solidi B 252 (2015) 1089–1095.
[19] Y. Chen, K. Zhang, M. Cao, S. Zhao, J. Zhang, X. Ma, Y. Hao, Study of surface leakage current of AlGaN/GaN high electron mobility transistors, Appl. Phys. Lett. 104 (2014) 153509.
[20] S. Zhou, H. Xu, B. Tang, Y. Liu, H. Wan, J. Miao, High-power and reliable GaN-based vertical light-emitting diodes on 4-inch silicon substrate, Opt. Express 27 (2019) A1506–A1516.
[21] M. Imura, K. Nakano, T. Kitano, N. Fujimoto, G. Narita, N. Okada, K. Balakrishnan, M. Iwaya, S. Kamiyama, H. Amano, I. Akasaki, K. Shimono, T. Noro, T. Takagi, A. Bandoh, Microstructure of epitaxial lateral overgrown AlN on trench-patterned AlN template by high-temperature metal-organic vapor phase epitaxy, Appl. Phys. Lett. 89 (2006) 221901.
[22] S. Hagedorn, A. Knauer, A. Mogilatenko, E. Richter, M. Weyers, AlN growth on nano-patterned sapphire: A route for cost efficient pseudo substrates for deep UV LEDs, Phys. Status Solidi A 213 (2016) 3178–3185.
[23] H. Fukuyama, H. Miyake, G. Nishio, S. Suzuki, K. Hiramatsu, Impact of high-temperature annealing of AlN layer on sapphire and its thermodynamic principle, Jpn. J. Appl. Phys. 55 (2016) 05FL02.
[24] H. Sun, S. Mitra, R.C. Subedi, Y. Zhang, W. Guo, J. Ye, M.K. Shakfa, T.K. Ng, B.S. Ooi, I.S. Roqan, Z. Zhang, J. Dai, C. Chen, S. Long, Unambiguously enhanced ultraviolet luminescence of AlGaN wavy quantum well structures grown on large misoriented sapphire substrate, Adv. Funct. Mater. 29 (2019) 1905445.
[25] S. Hagedorn, A. Knauer, F. Brunner, A. Mogilatenko, U. Zeimer, M. Weyers, High-quality AlN grown on a thermally decomposed sapphire surface, J. Cryst. Growth 479 (2017) 16–21.
[26] M.X. Wang, F.J. Xu, J.M. Wang, N. Xie, Y.H. Sun, B.Y. Liu, J. Lang, N. Zhang, W.K. Ge, X.N. Kang, Z.X. Qin, X.L. Yang, X.Q. Wang, B. Shen, The sapphire substrate pretreatment effects on high-temperature annealed AlN templates in deep ultraviolet light emitting diodes, CrystEngComm 21 (2019) 4632–4636.
[27] T.-Y. Wang, C.-T. Tasi, K.-Y. Lin, S.-L. Ou, R.-H. Horng, D.-S. Wuu, Surface evolution and effect of V/III ratio modulation on etch-pit-density improvement of thin AlN templates on nano-patterned sapphire substrates by metalorganic chemical vapor deposition, Appl. Surf. Sci. 455 (2018) 1123–1130.
[28] H. Chang, Z. Chen, W. Li, J. Yan, R. Hou, S. Yang, Z. Liu, G. Yuan, J. Wang, J. Li, P. Gao, T. Wei, Graphene-assisted quasi-van der Waals epitaxy of AlN film for ultraviolet light emitting diodes on nano-patterned sapphire substrate, Appl. Phys. Lett. 114 (2019) 091107.
[29] H. Long, J. Dai, Y. Zhang, S. Wang, B. Tan, S. Zhang, L. Xu, M. Shan, Z.C. Feng, H.-C. Kuo, C. Chen, High quality 10.6 μm AlN grown on pyramidal patterned sapphire substrate by MOCVD, Appl. Phys. Lett. 114 (2019) 042101.
[30] G. Bauer, W. Richter, Optical Characterization of Epitaxial Semiconductor Layers, Springer Science & Business Media, 2012.
[31] N. Okada, N. Kato, S. Sato, T. Sumii, T. Nagai, N. Fujimoto, M. Imura, K. Balakrishnan, M. Iwaya, S. Kamiyama, H. Amano, I. Akasaki, H. Maruyama, T. Takagi, T. Noro, A. Bandoh, Growth of high-quality and crack free AlN layers on sapphire substrate by multi-growth mode modification, J. Cryst. Growth 298 (2007) 349–353.
[32] M. Conroy, V.Z. Zubialevich, H. Li, N. Petkov, J.D. Holmes, P.J. Parbrook, Epitaxial lateral overgrowth of AlN on self-assembled patterned nanorods, J. Mater. Chem. C 3 (2015) 431–437.
[33] M.A. Moram, M.E. Vickers, X-ray diffraction of III-nitrides, Rep. Prog. Phys. 72 (2009) 036502.
[34] D.M. Follstaedt, N.A. Missert, D.D. Koleske, C.C. Mitchell, K.C. Cross, Plan-view image contrast of dislocations in GaN, Appl. Phys. Lett. 83 (2003) 4797–4799.
[35] G.G. Stoney, C.A. Parsons, The tension of metallic films deposited by electrolysis, Proc. R. Soc. London Ser. A 82 (1909) 172–175.
[36] B.W. Sheldon, A. Rajamani, A. Bhandari, E. Chason, S.K. Hong, R. Bereford, Competition between tensile and compressive stress mechanisms during Volmer-Weber growth of aluminum nitride films, J. Appl. Phys. 98 (2005) 043509.
[37] J.S. Tello, A.F. Bower, E. Chason, B.W. Sheldon, Kinetic model of stress evolution during coalescence and growth of polycrystalline thin films, Phys. Rev. Lett. 98 (2007) 21610.
[38] J.D. Acord, S. Raghavan, D.W. Snyder, J.M. Redwing, In situ stress measurements during MOCVD growth of AlGaN on SiC, J. Cryst. Growth 272 (2004) 65–71.
[39] A.E. Romanov, J.S. Speck, Stress relaxation in mismatched layers due to threading dislocation inclination, Appl. Phys. Lett. 83 (2003) 2569–2571.
[40] V.Y. Davydov, Y.E. Kitaev, I.N. Goncharuk, A.N. Smirnov, J. Graul, O. Semchinova, D. Uffmann, M.B. Smirnov, A.P. Mirgorodsky, R.A. Evarestov, Phonon dispersion and Raman scattering in hexagonal GaN and AlN, Phys. Rev. B 58 (1998) 12899.